

# Performance and limits of feedback cooling methods for levitated oscillators: a direct comparison

T. W. Penny, A. Pontin, and P. F. Barker\*

*Department of Physics and Astronomy, University College London,  
Gower St, London WC1E 6BT, United Kingdom*

(Dated: December 23, 2024)

Cooling the centre-of-mass motion is an important tool for levitated optomechanical systems, but it is often not clear which method can practically reach lower temperatures for a particular experiment. We directly compare the parametric and velocity feedback damping methods, which are used extensively for cooling the motion of single trapped particles in a range of traps. By performing experiments on the same particle, and with the same detection system, we demonstrate that velocity damping cools the oscillator to lower temperatures, it is also more resilient to imperfect experimental conditions. We show that these results are consistent with analytical limits as well as numerical simulations that include experimental noise.

## I. INTRODUCTION

Levitated nanoparticles in high vacuum are thermally and mechanically well isolated from the environment. Both classical and quantum harmonic oscillators can be created without the need for cryogenic operation. They can be cooled from room temperature to low occupancy, or even to the groundstate, via cavity or feedback cooling [1–3]. Levitated oscillators are increasingly seen as ideal candidates for tests of fundamental quantum mechanics with proposed experiments to create large mass superpositions via matter-wave interferometry [4–6] or to study mechanisms of wavefunction collapse [7, 8]. Levitated nanoparticles have also been used for weak force measurements [9] with direct measurements of photon recoil [10], and even for testing the standard model [11].

Controlling the motion of levitated nanoparticles has seen much interest in the last decade, particularly in cooling the centre-of-mass (CoM) temperature towards the ground state [12, 13]. This is seen as a milestone in gaining full quantum control of macroscopic objects and is an initial step in matter-wave interferometry protocols [14]. Cooling the motion of a trapped nanoparticles to even fairly modest temperatures can be useful for preventing particle loss in high vacuum [9, 15].

Ground state cooling has been achieved using coherent scattering from an optical tweezer into a cavity mode to remove energy from the particle motion [1]. Previous attempts to cool trapped nanoparticles have included other forms of cavity cooling utilising direct trapping in the cavity [16] and hybrid traps [17]. An alternative method is feedback cooling based on measurements of the trapped particle motion. Modulating the trapping potential at twice the particle frequency (parametric feedback) or applying a linear force proportional to the particle’s velocity (velocity damping) are two techniques that have been used extensively. Average phonon occupancies of 62.5 phonons [18] and 0.56 phonons [2] have been

achieved respectively in optical tweezer set-ups using this type of cooling.

As both techniques are commonly used, it is natural to ask which is likely to achieve lower temperatures from both a theoretical and experimental perspective. In this paper we directly compare parametric feedback cooling and velocity damping for a particle confined in a Paul trap. Parametric feedback is implemented by tracking the instantaneous phase of the trapped particles using a phase-locked loop (PLL) and modulating the trapping potential with a frequency-doubled signal phase-locked to the particle motion with an appropriate phase shift. This implementation is commonly used in optical traps [18, 19] but this is the first time it has been realised in a Paul trap. Velocity damping is achieved by measuring the position of the particle as a function of time which is subsequently used to estimate velocity which is then utilised as the feedback signal. We have taken common concepts from PLL theory and applied these to the optomechanical system to set bounds on the minimum temperatures achievable with parametric cooling using a PLL. Both cases of cooling are simulated and experimentally demonstrated on the same particle under identical experimental conditions. We consider the minimum achievable temperature of each method and discuss the implications of experimental imprecision. Finally, we examine the energy distributions of the cooled oscillator.

## II. FEEDBACK COOLING SCHEMES

A levitated nanoparticle can be considered a thermal oscillator in a 3D harmonic potential. The motion in each direction  $x_i$ , where  $i = \{x, y, z\}$ , obeys an equation of motion given by:

$$\ddot{x}_i + \gamma_0 \dot{x}_i + \omega_i^2 x_i = \frac{F_{th,i}}{m}, \quad (1)$$

where  $\gamma_0$  is gas damping,  $\omega_i$  is the frequency of oscillation,  $m$  is the mass of the trapped particle and  $F_{th}$  is a random Langevin force that satisfies  $\langle F_{th,i}(t)F_{th,j}(t') \rangle =$

\* p.barker@ucl.ac.uk

$2m\gamma_0k_BT_0\delta(t-t')\delta_{i,j}$  where  $k_B$  is the Boltzmann constant and  $T_0$  is the temperature of the surrounding thermal bath. The CoM temperature of the particle can be estimated using the variance of the motion,  $T_{CoM} = m\omega_i^2\langle x_i^2 \rangle/k_B$ . With no additional forces being applied to the particle it is equal to the temperature of the surrounding thermal bath i.e.  $T_{CoM} = 293K$ .

Without loss of generality the equations of motion can be considered in 1D with similar equations applying to all directions. The effect of the interactions between modes are considered later. Velocity damping cools an oscillator by applying a force proportional to the velocity to increase the damping. However, any noise in the detection will also be fed back to the oscillator. Eq. 1 can be modified to include these effects such that [20]:

$$\ddot{x} + \gamma_0\dot{x} + \omega_0^2x = \frac{F_{th}}{m} - \gamma_{fb}(\dot{x} + \delta\dot{x}), \quad (2)$$

where  $\gamma_{fb}$  is the damping due to feedback,  $\omega_0 = \omega_x$ , and  $\delta\dot{x}$  is a stochastic, additive noise in the feedback signal.

Parametric feedback cools a trapped particle by modulating the trapping potential at twice the frequency of the particle motion. The modulation can be created by multiplying the current position and velocity together,  $x(t)\dot{x}(t)$  [21]. This scheme is often implemented using a digital PLL to lock a numerically controlled oscillator (NCO) to the phase of the particle then frequency doubling an output from the NCO to use as the feedback signal (with an appropriate phase shift) [18]. Although both are considered parametric feedback these two implementations produce different particle dynamics because the feedback signal from a PLL has a constant amplitude whereas the amplitude of the feedback from multiplying position and velocity is dependent on particle energy [22, 23]. The equation of motion of the oscillator under parametric feedback with a PLL is:

$$\ddot{x} + \gamma_0\dot{x} + (1 - G\sin(2(\omega_0t + \theta_0)))\omega_0^2x = \frac{F_{th}}{m}, \quad (3)$$

where  $G$  is the modulation depth and  $\theta_0$  is a time dependent phase set by the PLL. Fig. 1 shows a schematic of a general digital PLL with a breakdown of the phase detector to show how it is implemented in the simulation and experiment. Signals from the NCO and the oscillator are fed into a phase detector which produces an output proportional to the phase difference between the two signals with a constant of proportionality,  $K_d$ . A loop controller is applied to the output then multiplied by a gain constant,  $K_o$ , to produce the control signal for the NCO. By modifying the controller transfer function and gain constant, the PLL can be made to accurately track the phase by minimising the phase detector output. Despite being digitally implemented we will consider all transfer functions in their analogue equivalent form for the purposes of analysis. This is valid because all features of an analogue transfer function appear in the digital equivalent.

### III. SIMULATION

The simulations are implemented using the energy conserving (symplectic) leapfrog method [24]. Eq. 1, with an additional feedback force, is rewritten as a system of two first order equations:

$$\dot{x} = v \quad (4)$$

$$\dot{v} = -\gamma_0v - \omega_0^2x + \frac{1}{m}(F_{th} + F_{fb}) \quad (5)$$

and each variable is progressed one half-timestep out of sync:

$$x_{n+1} = x_n + v_{n+\frac{1}{2}}\Delta t \quad (6)$$

$$v_{n+\frac{1}{2}} = v_{n-\frac{1}{2}} + \dot{v}_n\Delta t \quad (7)$$

where  $\Delta t$  is the timestep size in the simulation. Thermal force noise and measurement noise are simulated using a string of random numbers with a Gaussian distribution and variance equal to  $(2k_BT_0\gamma_0)/(m\Delta t)$  and  $S_{nn}/\Delta t$  respectively where  $T_0$  is the temperature of the surrounding thermal bath and  $S_{nn}$  is the detection noise spectral density which is assumed to be uncorrelated and white. The gas damping is pressure dependent obeying the equation  $\gamma_0 = (1 + \frac{\pi}{8})\frac{4\pi}{3}\frac{MNR^2v_T}{m}$  where  $M$  is the gas molecular mass,  $N$  is the pressure dependent gas particle density,  $R$  is the sphere radius and  $v_T = \sqrt{\frac{8k_BT_0}{\pi M}}$  is the average thermal velocity of the air molecules [25].

Two methods to generate the feedback signal for velocity damping were considered. The first method uses a Wiener filter [26, 27]. Wiener filtering allows us to extract the best estimation of a variable from a noisy measurement of a related variable provided we have knowledge of the transfer function of the system. More explicitly if we measure position,  $x$ , with additional noise in order to estimate velocity,  $v$ , where  $x$  and  $v$  are related in via  $S_{xx}(\omega) = \frac{1}{\omega^2}S_{vv}(\omega)$  then the optimum filter is given by [26]:

$$W(\omega) = \frac{\omega}{1 + \frac{S_{nn}(\omega)}{S_{xx}(\omega)}}. \quad (8)$$

A caveat is that Wiener filtering only works for stationary processes, which is not strictly true when cooling a harmonic oscillator, since the transfer function is altered by the cooling process. However, the process is only non-stationary during the transient period of cooling therefore the transfer function of the steady state can be calculated using the applied feedback gain and used when computing the Wiener filter. By applying the Wiener filter to a time-dependent position measurement

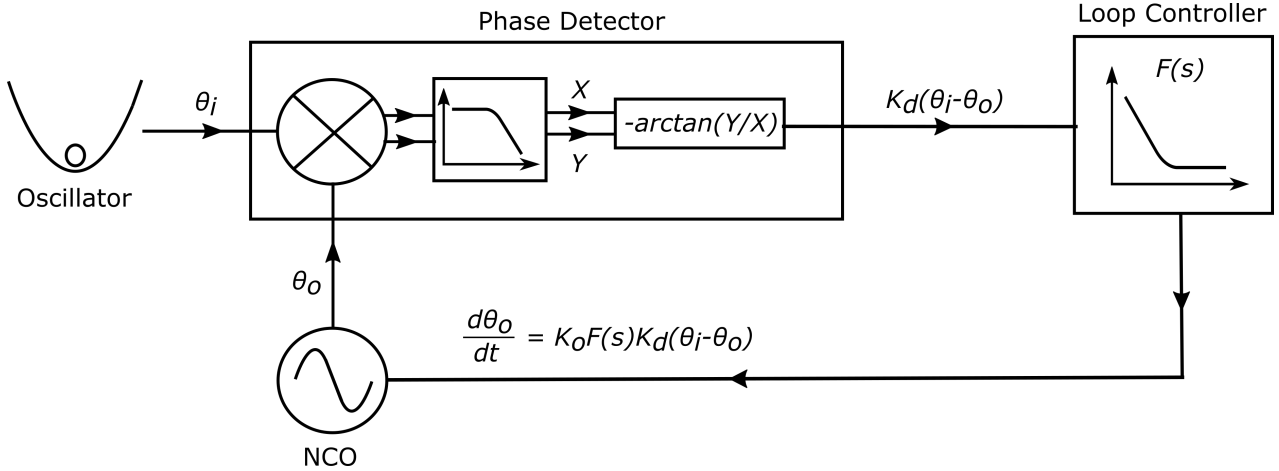


FIG. 1. A basic digital PLL loop consists of a NCO that tracks the oscillator phase through an input that alters the frequency. A phase detector takes both the oscillator and NCO signals as inputs and produces an output proportional to the phase difference. In the simulation and experiment the phase detector mixes the signals to produce X and Y quadratures of the oscillator signal. Low-pass filters are used to remove noise and the  $2\omega_0$  component. The X and Y quadratures can then be used to calculate the phase difference between the NCO and oscillator. The digitally implemented loop controller, with an an equivalent analogue transfer function  $F(s)$ , is adjusted such that the NCO tracks the phase of the oscillator. The NCO acts as an integrator and must be considered when calculating the closed-loop transfer function.

the velocity can be estimated. Alternatively, the velocity can be predicted by delaying the measured position signal by  $\frac{\pi}{2\omega_0}$  seconds. This method is valid under the high-Q approximation, where  $\omega \approx \omega_0$  over the width of the transfer function. The estimated velocity from either method can then be used as the feedback signal.

For parametric feedback, a digital PLL was implemented in the simulation. A sinusoidal function with direct access to the phase is used as the NCO. The phase of the oscillator at each timestep is calculated by demodulating the current oscillator position (with added measurement noise) with the signal from the NCO to obtain the  $X$  and  $Y$  quadratures. Filtering the quadratures using second-order exponential smoothing, with a bandwidth  $B_{quad}$ , removes the  $2\omega_0$  component of the signal allowing the phase difference to be calculated using  $\delta\theta = -\arctan(Y/X)$ . We use  $K_d = K_o = 1$  in the simulation. To generate a control signal in the simulation we use a loop controller with a transfer function of:

$$F(s) = -\left(\frac{\tau_2}{\tau_1} + \frac{1}{\tau_1 s}\right) \quad (9)$$

where  $\tau_1$  and  $\tau_2$  are the two time-constants of the filter. This form of the transfer function demonstrates its equivalence to a PI loop. This is one of the most widely employed loop controllers in PLLs and provides a balance between narrow bandwidth and loop stability [28]. Implementing a digital filter of the form  $G(s) = -F(s)/s$  gives the open-loop transfer function. Using this we can directly calculate a new phase,  $\theta_o$ , for our NCO from the phase detector output. It is useful to note that the closed-loop transfer function becomes [28]:

$$\frac{\theta_o}{\theta_i} = H(s) = \frac{2\omega_n \zeta s + \omega_n^2}{s^2 + 2\omega_n \zeta s + \omega_n^2} \quad (10)$$

where  $\omega_n = \sqrt{\frac{K_o K_d}{\tau_1}}$  and  $\zeta = \frac{\tau_2}{2} \sqrt{\frac{K_o K_d}{\tau_1}}$  are the natural frequency and the damping factor of the PLL. The PLL bandwidth can be defined using the 3dB cut-off of the closed-loop transfer function [28]:

$$B_{3dB} = \omega_n [2\zeta^2 + 1 + \sqrt{(2\zeta^2 + 1)^2 + 1}]^{\frac{1}{2}}. \quad (11)$$

This determines the rate of change of the oscillator phase that can be tracked by the PLL.

#### IV. THEORETICAL ANALYSIS

Eq. 2 can be solved to find the variance of the oscillator. Making the high-Q approximation, which is valid at low pressures, the CoM temperature of the oscillator is calculated as [20, 29]:

$$T_{CoM} = T_0 \frac{\gamma_0}{\gamma_0 + \gamma_{fb}} + \frac{1}{2} \frac{m\omega_0^2}{k_B} \frac{\gamma_{fb}^2}{\gamma_0 + \gamma_{fb}} S_{nn} \quad (12)$$

where the second term gives the contribution from the detection noise. Physically this results from noise in the measurement being fed into the motion of the particle causing heating. This also leads to a phenomenon known as noise squashing where correlations between detection noise and particle motion make the power spectral

density (PSD) of the particle motion from the detector being used to generate the feedback signal (in-loop detector) appear as if it is being cooled below the noise floor [20, 30]. In the limit  $\gamma_{fb} \gg \gamma_0$  the optimum feedback gain provides an effective damping given by:

$$\gamma_{fb}^{opt} = \sqrt{\frac{2\gamma_0 k_B T_0}{S_{nn} m \omega_0^2}} \quad (13)$$

with a minimum temperature of:

$$T_{CoM}^{vmin} = \sqrt{\frac{2S_{nn} m \omega_0^2 \gamma_0 T_0}{k_B}}. \quad (14)$$

In contrast to velocity damping, a theoretical analysis of the PLL is extremely difficult when adding noise into the closed-loop due to the non-linear nature of the PLL. A limited analysis can be done using a simplified loop controller with only proportional control,  $F(s) = P$  where  $P$  is a constant, and the assumption of small phase error,  $\sin(\delta\theta) = \delta\theta$  [22, 31]. In this regime the temperature of the oscillator is still decoupled from variations in phase error and we cannot predict the effect of detection noise on the oscillator temperature. However, it can be shown that the bandwidth of the PLL limits the modulation depth,  $G$ , that can be applied whilst still maintaining phase tracking according to:

$$G_{lim} = \frac{2B_{3dB}}{\omega_0}. \quad (15)$$

In Fig. 2a) we show the temperature of a simulated oscillator being cooled parametrically for a range of  $\zeta$  and  $\omega_n$  values at a fixed modulation depth. To reflect the experimental conditions in our set-up, a particle radius of  $R = 193.5$  nm and density  $\rho = 1850$  kg m<sup>-3</sup> is used. The oscillator frequency is set to be  $\omega_0 = 2\pi \times 277$  Hz with a pressure of  $P = 2.3 \times 10^{-6}$  mbar giving an intrinsic linewidth of 780  $\mu$ Hz. The detection noise spectral density is  $S_{nn} = 1.5 \times 10^{-17}$  m<sup>2</sup> Hz<sup>-1</sup>. The quadrature filter bandwidth,  $B_{quad}$ , is fixed at  $2\pi \times 400$  Hz for all parameter values so that it is much larger than any  $B_{3dB}$  values used and does not interfere with the PLL loop controller.

Provided  $\zeta$  is large enough there is an optimum value of  $B_{3dB} = 2\pi \times 104$  Hz that is unaffected by individual  $\zeta$  and  $\omega_n$  values. The large  $\zeta$  limit is the equivalent of large DC loop gain being required for good tracking [28]. From now on we can just consider the PLL to contain three parameters  $B_{quad}$ ,  $B_{3dB}$  and  $G$ . The quadrature filter bandwidth must be large enough so that it does not interfere with the loop controller but it must be sufficiently small to eliminate the  $2\omega_0$  component in the demodulated signal. We find that keeping  $B_{quad} = 5B_{3dB}$  is sufficient. For larger bandwidths this makes it impossible to completely remove the  $2\omega_0$  component from the demodulated signal, however, the PLL still tracks and

cools the oscillator. This leaves only two independent parameters to adjust,  $G$  and  $B_{3dB}$ .

We show in Fig. 2b) the temperature of a cooled oscillator as the modulation depth is adjusted for several different PLL bandwidths. It can be seen that for each bandwidth there is an optimum gain that increases as the bandwidth is increased as predicted by Eq. 15. Heuristically, this results from the linewidth of the oscillator increasing as it is cooled. Once the linewidth is larger than the PLL bandwidth the particle phase can no longer be tracked consistently so the phase error increases and the particle is cooled less effectively. This is confirmed in Fig. 2c) which shows the linewidth of a cooled oscillator at optimum gain for several PLL bandwidths. A straight line fit to the first four points gives a gradient of 0.6 suggesting the PLL struggles to track the oscillator even when the linewidth is less than  $B_{3dB}$  due to the more complex loop controller and large phase error. Similar trends to those in Fig. 2 are seen for alternative pressures, oscillator frequencies and particle masses. Using Eq. 15 we can calculate an achievable temperature at any particular bandwidth, this is given by:

$$T_{CoM}^{lim1} = T_0 \frac{\gamma_0}{B_{3dB}} = T_0 \frac{2\gamma_0}{G_{lim} \omega_0}. \quad (16)$$

These simulations show the modulation depth is not limited to 1% as previously reported for optical traps [32]. We found the modulation depths were also not limited by this value in the experiment where modulation depths of up to 5% were used. Fig. 2b) additionally shows the bandwidth cannot be indefinitely increased without incurring a penalty on the effectiveness of the PLL. For a sinusoidal input into the PLL with amplitude  $V_s$ , the loop SNR can be defined as  $SNR_L = \frac{V_s^2/2}{2B_L S_{nn}}$  [28] where  $B_L$  is the noise bandwidth of the loop (in hertz). For the loop controller used in this numerical simulation  $B_L = \frac{1}{2}\omega_n(\zeta + \frac{1}{4\zeta})$ . If the SNR drops below  $\sim 1$  then the loop will completely lose lock and require the SNR to increase several decibels before the loop can lock again [28]. If we redefine the SNR for a thermal oscillator by naively replacing the numerator with the position variance then it becomes  $SNR_L = \frac{\langle x^2 \rangle}{2B_L S_{nn}}$ . We can then define the lower bound the temperature of the oscillator can reach before the PLL unlocks as:

$$T_{CoM}^{lim2} = \frac{m\omega_0^2}{k_B} 2B_L S_{nn}. \quad (17)$$

These two limits allow us to bound the smallest achievable temperature of the oscillator during parametric feedback cooling. Note that unlike Eq. 12 they are not a complete analytical expression for the temperature but bounds on what can be achieved since they do not include the effect of phase noise on the temperature, i.e., the model does not include the backaction of the feedback scheme. Furthermore, in the derivation of Eq. 17 we have

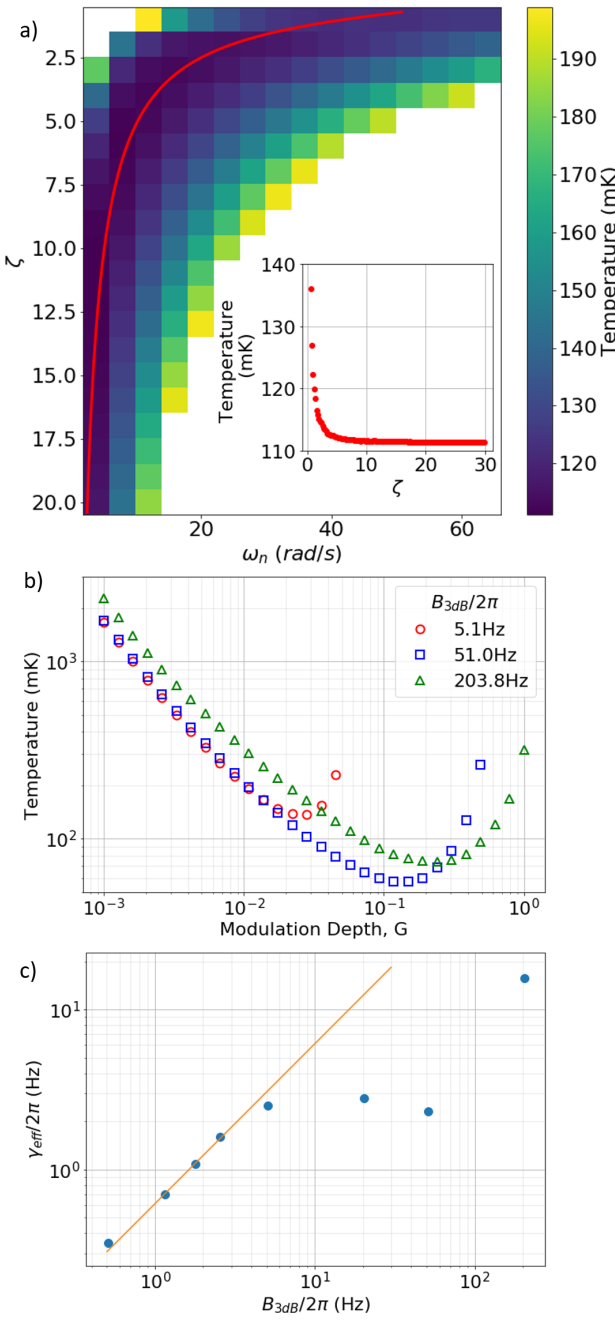


FIG. 2. a) Heatmap showing the CoM temperature for parametric cooling with different  $\omega_n$  and  $\zeta$  parameters. The red line shows a constant bandwidth of 104 Hz along which the temperature is at a minimum. The inset shows the temperature variation along the red line. b) Temperature of a parametrically cooled oscillator against modulation depth for several different PLL bandwidths. c) The linewidth of the cooled oscillator at the optimum gain against the bandwidth. The orange line shows a straight line fit to the first four data points with a gradient of 0.6.

exchanged a constant amplitude signal for a signal with a varying amplitude and considered only the average. In reality, the PLL often tracks the signal on a much shorter

timescale than the evolution of the oscillator amplitude. Therefore, if at any point during the measurement the instantaneous loop SNR drops below 1 the PLL will unlock and the oscillator temperature will increase. This means that in practice the oscillator will never reach the temperature given by Eq. 17, however, it can never be significantly lower than this. We can use these bounds to predict a bandwidth at which the minimum temperature will occur. Using the relation  $B_{3dB} \approx 8\pi B_L$  (valid in the limit  $\zeta^2 \gg 1$ ) we find the optimum bandwidth for cooling is:

$$B_{3dB}^{opt} = \sqrt{\frac{4\pi\gamma_0 k_B T_0}{S_{nn} m \omega_0^2}}. \quad (18)$$

Using equation 16 the minimum achievable temperature is:

$$T_{CoM}^{PLLmin} = \sqrt{\frac{S_{nn} m \omega_0^2 \gamma_0 T_0}{4\pi k_B}} \quad (19)$$

which is lower than of the minimum temperature that can be achieved with velocity damping. This is because the model for velocity damping includes backaction from the noise in the feedback whereas the model for the parametric feedback does not. Simulations must be used to fully include the effects of noise from the PLL on the particle motion as shown below.

## V. EXPERIMENT

Paul traps utilise an alternating electric field to trap charged particles since Gauss' Law forbids a minimum for three-dimensional static electric fields in free space. For a linear Paul trap the potential is [33]:

$$\Phi(x, y, z, t) = U_0 \frac{\kappa}{z_0^2} \left( \frac{x^2 + y^2}{2} + z^2 \right) + \frac{V_0}{2} \cos(\omega_{rf} t) \left( \eta \frac{x^2 - y^2}{r_0^2} + 1 \right) \quad (20)$$

where  $U_0$  is the DC voltage applied to the electrodes,  $V_0$  is the AC voltage applied to the electrodes at angular frequency  $\omega_{rf}$ , and the parabolic coefficients  $r_0$ ,  $z_0$ ,  $\kappa$  and  $\eta$  are determined by the geometry of the trap. In the case of no damping the particle motion in one-dimension can be approximated to [34]:

$$x_i(t) \approx 2AC_0 \cos(\omega_i t) \left( 1 - \frac{q_i}{2} \cos(\omega_{rf} t) \right) \quad (21)$$

where  $A$  is determined by the initial conditions of the particle,  $C_0$  is a function of particle and trap parameters,  $\omega_i \approx \frac{\omega_{rf}}{2} \sqrt{a_i + \frac{q_i^2}{2}}$  is the 'secular frequency' and  $a_i$

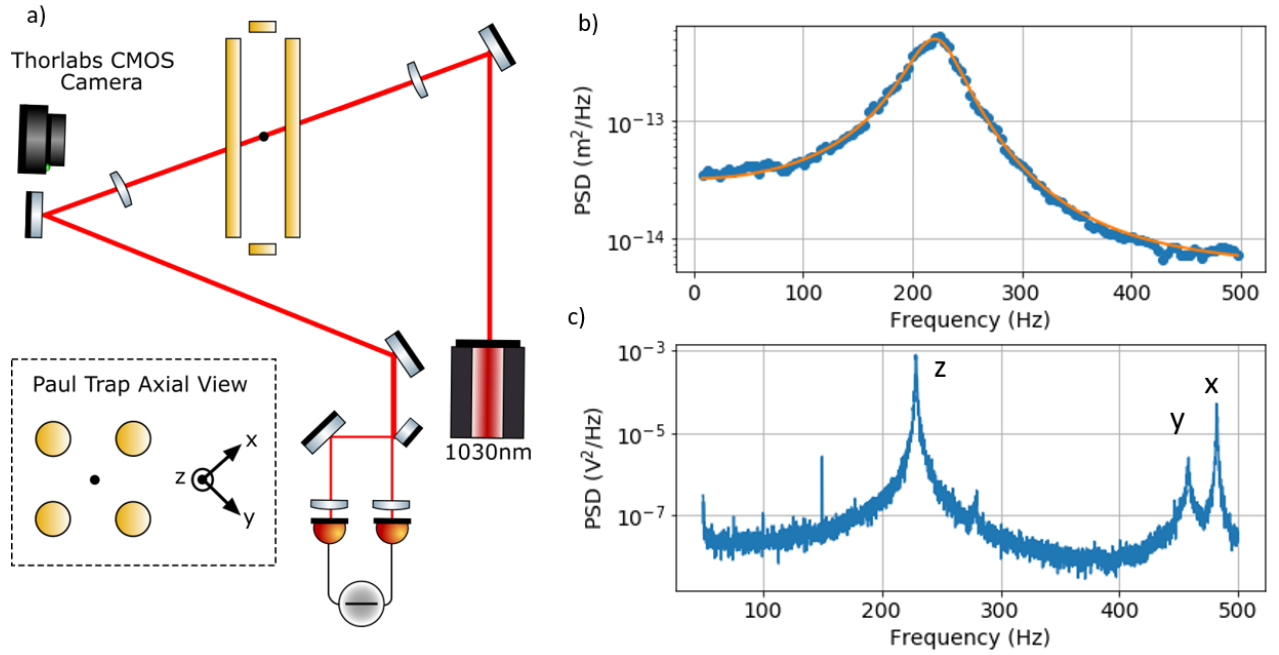


FIG. 3. a) Simplified experimental set-up. A focused 1030 nm laser illuminates the particle. The scattered light can be captured and focused onto a CMOS camera to track the motion. The forward scattered and unscattered light is also collected and focused onto balanced photodiodes to generate the signal used in the feedback electronics. b) PSD of the particle used in this experiment with  $\omega_z = 2\pi \times 223$  Hz taken with CMOS camera at  $1.9 \times 10^{-1}$  mbar with fit (orange line). The variance of the PSD gives a particle mass of  $5.3 \pm 0.3 \times 10^{-17}$  kg. c) Spectrum measured on the balanced detection at  $2.2 \times 10^{-3}$  mbar showing all three modes of motion during cooling. The modes have frequencies  $\omega_x = 2\pi \times 482$  Hz,  $\omega_y = 2\pi \times 450$  Hz, and  $\omega_z = 2\pi \times 229$  Hz. The spectrum is left uncalibrated since each mode requires separate calibration.

and  $q_i$  are known as the stability parameters of the trap. The stability parameters are given by  $q_x = q_y = \frac{2qV_0\eta}{m\omega_{rf}^2r_0^2}$ ,  $q_z = 0$  and  $a_x = a_y = -0.5a_z = \frac{4qU_0\kappa}{m\omega_{rf}^2z_0^2}$ . For this approximation to hold the conditions  $|a_i|, q_i \ll 1$  must be met. Eq. 21 describes a harmonic 'secular' motion with frequency  $\omega_i$  and a smaller, driven 'micromotion' at higher frequencies,  $\omega_{rf} \pm \omega_i$  [34].

The Paul Trap used in this experiment consisted of four parallel rods held by printed circuit board (PCB) similar to the trap in reference [35]. The PCB allowed for easy electrical connections to the rods and had two ring electrodes etched into the surface as endcaps to confine the particle along the trap axis. The PCB was gold coated to minimise charge build up causing stray fields around the trap. For this trap the geometric factors are  $r_0 = 1.1$  mm,  $z_0 = 3.5$  mm,  $\kappa = 0.071$  and  $\eta = 0.82$ . Typical voltages and trap frequencies used were  $V_0 = 100 - 400$  V,  $U_0 = 50 - 150$  V and  $\omega_{rf} = 2\pi \times 4 - 8$  kHz.

Silica nanoparticles were loaded into the trap at approximately  $7 \times 10^{-2}$  mbar using the electrospray technique with a quadrupolar guide [35] and can be pumped down to low pressures without feedback. Individual nanospheres could be easily charged to approximately 1500 elementary charges with this method. Trapped particles were detected visually on a CMOS camera using scattered light from a 1030 nm diode laser.

The radius of the trapped particle could be determined using the CMOS camera to track the motion of the particle [35, 36]. Fig. 3b) shows a PSD of the particle motion in the  $z$ -direction at a pressure of  $1.9 \times 10^{-1}$  mbar. Assuming a CoM temperature of 293 K and density of  $1850 \text{ kg m}^{-3}$ , a radius of  $190 \pm 4$  nm was determined. This agrees with the expected 193.5 nm radius of the silica particles that were nominally being trapped. This particle has a charge-to-mass ratio of  $\sim 1.2 \text{ C kg}^{-1}$  corresponding to  $\sim 421$  charges.

Real time detection of the particle motion was done using balanced photodiodes as shown in Fig. 3a). All three modes of motion have a projection perpendicular to the laser beam and therefore motion along all axes can be detected using a single balanced detector (spectra shown in Fig. 3c)). The signal from the balanced photodiodes can be sent directly to either a PLL or FGPA to generate the feedback signal. The balanced detector can be calibrated for the  $z$ -mode by acquiring timetraces on both the balanced detector and the CMOS camera simultaneously then comparing the variance in the  $z$ -mode. This can be done at any pressure so does not require the assumption that the calibration remains constant at all pressures unlike calibration by assuming thermal equilibrium at a high pressure [37]. For balanced detection the laser was typically focused onto the particle with an intensity of  $1.27 \times 10^7 \text{ W m}^{-2}$ . Increasing the laser inten-

sity by a factor of 3 was found to have no effect on the frequency or position of the particle therefore at these intensities any effect to the particle motion can be considered negligible.

A Red Pitaya FGPA was used to generate the feedback signal for the velocity damping scheme using the IQ module in the PyRPL software package. A signal proportional to the measured motion of the particle with an arbitrary delay and gain could be produced. Other modes in the feedback signal were found to couple to the particle motion and cause heating. To prevent this the input signal was filtered around the appropriate spectral peak. The  $x$ - and  $y$ -modes were cooled by adding a signal to an appropriate rod of the Paul trap such that the force opposes the particle motion. The  $z$ -mode was cooled by applying the feedback to one of the endcaps using electronics built in-house.

A Zurich Instruments HF2LI lock-in amplifier was used as a PLL to generate the feedback signal for parametric feedback cooling. The loop controller parameters of the PLL were automatically generated by the lock-in amplifier based on a user defined bandwidth. The signal from a frequency doubled NCO with continuously tunable phase could be output as the modulation signal. The  $z$ -mode was cooled by modulating both endcaps using electronics built in-house with a maximum modulation depth of 5%.

Although we only consider the temperature of the  $z$ -mode, the  $x$ - and  $y$ -motion of the particle was cooled using velocity damping throughout the experiment. This minimises the cross-coupling between modes and improves the noise floor of the CMOS camera detection. The feedback on the  $z$ -mode could easily be switched between parametric cooling and velocity damping without losing the trapped particle.

## VI. COOLING

Fig. 4a) shows the CoM temperature against damping rate for velocity damping in both the experiment and simulations alongside the analytical results. Experimentally, cooling was performed on the  $z$ -mode of the oscillator with a frequency of  $\omega_z = 2\pi \times 277$  Hz at a pressure of  $2.3 \times 10^{-6}$  mbar with an expected intrinsic linewidth of  $780 \mu\text{Hz}$ . The simulations were performed with the same parameters using the experimentally measured detection noise spectral density of  $S_{nn} = 1.5 \times 10^{-17} \text{ m}^2 \text{ Hz}^{-1}$  and nominal particle radius and density of  $R = 193.5 \text{ nm}$  and  $\rho = 1850 \text{ kg m}^{-3}$ . The red, cyan and dark blue lines show the first term, second term and total in Eq. 12 respectively. The black circles show the simulation results where the Wiener filter described by Eq. 8 is used to estimate the velocity based on a measurement of the particle position that includes detection noise. These results agree with the analytical results across all feedback gains. The result of using a delayed position signal as a feedback signal are shown by the purple circles. Using an additional bandpass filter to remove detection noise in

the feedback signal similar to the experiment makes no difference to the CoM temperatures in this case. For low feedback gains the simulation temperatures agree with the analytical results and are lower than when using an optimum Wiener filter. This is due to phase delays in the Wiener filter. For large feedback gains the simulation begins to heat more than expected. This is because as the effective damping increases  $\omega$  can no longer be assumed constant over the oscillator linewidth and the assumption of high-Q is no longer valid. Simulations were run for feedback gains higher than 200 Hz but the oscillator temperature was significantly higher than 1 K so are not shown. Although here both schemes for generating a feedback signal achieve similar minimum temperatures, as the Q-factor of the oscillator decreases the Wiener filter technique will cool to lower temperatures. For example, for a 70 nm particle at the same pressure and oscillation frequency ( $\gamma_0 = 2.1 \text{ mHz}$ ), the Wiener filter technique achieves a lower temperature by a factor 2. The experimental results (green circles) agree well with the simulation and analytical prediction at all feedback gains with a minimum temperature of  $26 \pm 6 \text{ mK}$  attained. The maximum experimentally achievable gain was used and is shown on the graph. At the maximum gain the experiment appears to still follow the analytical result despite using the delayed position as the feedback signal. A higher gain would be required to show conclusively whether this feedback method deviates from the analytical result as seen in the simulation. By reducing the pressure further we predict temperatures comparable to those shown in previous Paul Trap experiments [38].

CoM temperature against PLL bandwidth for parametric cooling of the oscillator are shown in Fig. 4b) for the experiment, simulation and analytical bounds. Parametric feedback was performed on the same trapped particle with identical experimental parameters as velocity damping. Eq. 16 and Eq. 17 are shown by the red and cyan lines respectively. The black circles show the results of the simulations using the model described previously where only one dimension is considered with white detection noise. For low bandwidths the simulation cannot cool as low as the analytical bound. This is due to the more complicated loop controller and phase noise preventing the PLL tracking the oscillator up to the PLL bandwidth. However, the temperature is still inversely proportional to  $B_{3dB}$  as predicted. The simulation deviates from this trend as  $B_{3dB}$  increases due to greater phase noise in the NCO arising from the smaller detection SNR at lower temperatures. It can be seen that the temperature begins to increase for higher bandwidths as the PLL begins to unlock due to low  $SNR_L$ . The experiment (green circles) shows higher temperatures than the simulation for all bandwidths with a minimum temperature of  $280 \pm 20 \text{ mK}$ . This is lower than previously achieved by parametric feedback in a Paul trap [39, 40]. Once the bandwidth increases above 100 Hz (the grey region in Fig. 4b)) the PLL begins to lose lock and the oscillator becomes unstable. In the experiment a quadrature

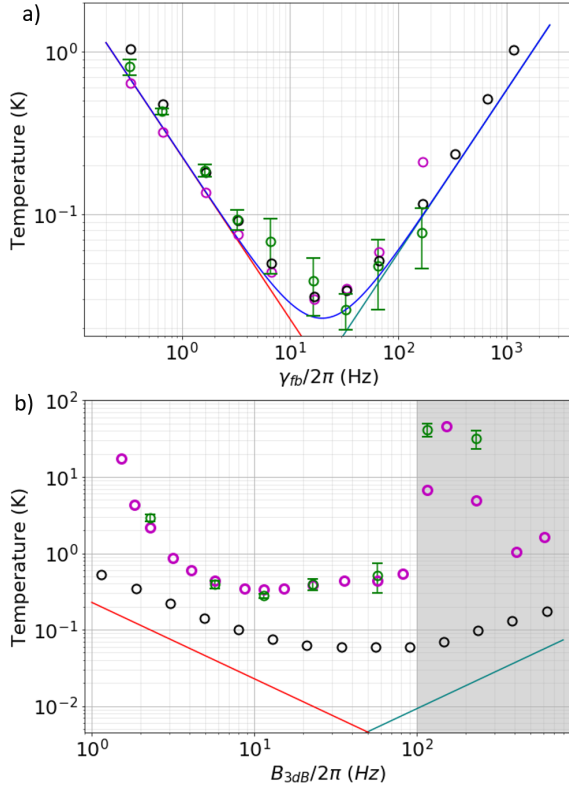


FIG. 4. Analytical, simulation and experimental results of cooling the axial motion of the particle. Experimentally both cooling schemes were done on the same particle with the same detection parameters. The frequency of motion was 277 Hz. a) Cooling with velocity damping. Green circles are experimental data, black circles are simulation using a Wiener filter to predict the velocity and magenta circles are simulation where a delayed position signal predicts the velocity. The red and teal lines show the first and second terms in Eq. 12 respectively and the blue line shows the total. b) Cooling with parametric feedback via a PLL. Green circles are experimental data, black circles are the ideal simulation and magenta circles are the improved model simulation. The red line represents Eq. 16 and the teal line represents Eq. 17. The shaded region shows when the PLL begins to unlock from the oscillator in the experiment. For both parametric feedback and velocity damping the modulation was experimentally increased to the maximum gain.

bandwidth of  $B_{quad} = 5B_{3dB}$  was used based on the simulation results. To begin to understand what limited the final temperature of the experiment an improved model was designed to more realistically simulate the experiment. The modulation depth is limited to 5% to match the experimental limit. Due to instabilities in the amplitude and frequency of the trap potential the frequency of the particle experiences a smooth drift [41]. This is approximated by a slow sinusoidal modulation of the oscillator frequency in the model and increases the CoM temperature for low bandwidths where the modulation is bigger than or comparable to  $B_{3dB}$ . As seen in Fig. 3c), other modes of motion appear in the detection signal

which the PLL can lock to at high bandwidths causing modulation at the wrong frequency and heating the particle. These can be added to the simulation along with second-order harmonics to match experimental spectra. Additionally, shifting the particle away from the trap centre introduces a driving force from the feedback signal and heats the particle due to noise in the feedback signal. Finally, the lock-in amplifier used experimentally has a 'range' feature that was included in the improved model. This limits the frequency difference between the NCO and the oscillator. The purple circles in Fig. 4b) show the results of this improved model. Much better agreement is now seen between the simulation and experiment below 100 Hz. Once  $B_{3dB}$  is increased above this in the simulation the range feature starts having a large impact on the dynamics and prevents the PLL from completely unlocking.

The lowest experimentally achieved temperature was an order of magnitude lower for velocity damping than parametric cooling with the PLL. Our simulations show that this is partly due to other modes in the detection signal, a drift of the central frequency of the oscillator and the particle being offset from the centre of the trap which do not affect the velocity damping scheme. This is because velocity damping acts on the particle from one direction therefore any changes in position can be compensated for by a change in the feedback gain. In addition, any changes to the central frequency are automatically tracked since the position measurement is used as the feedback signal and other frequencies in the detection signal do not couple to the  $z$ -mode. Even in the case with only one mode and white noise in the detection the simulation shows the backaction on the particle due to measurement noise is larger for PLL parametric feedback than for velocity damping. Similar trends are seen at alternative pressures, particle radii and oscillator frequencies.

## VII. ENERGY DISTRIBUTIONS

A trapped nanoparticle obeying Eq. 1 is expected to have an energy distribution given by the Boltzmann-Gibbs (thermal) distribution:

$$\rho(E) = \frac{1}{Z_\alpha} e^{-\frac{E}{k_B T_0}} \quad (22)$$

where  $Z_\alpha$  is the normalisation constant such that  $\int_0^\infty \rho(E)dE = 1$ . By adding feedback to the oscillator we can expect to alter the dynamics and change the energy distribution of the particle.

In the case of velocity damping and PLL parametric feedback we can use the Stratonovitch-Kaminskii Limit theorem to write a Fokker-Plank equation and calculate the distributions [22, 43, 44]:

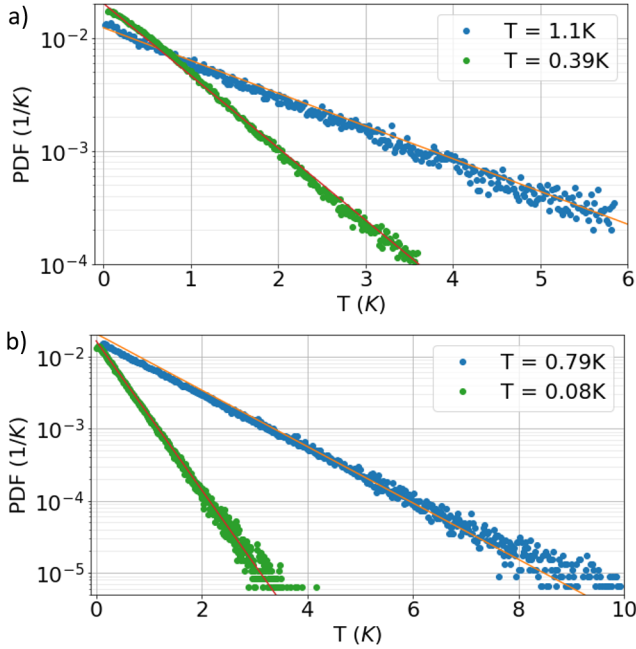


FIG. 5. Energy distribution for experimental data in units of  $k_B$ . a) Distributions from a parametrically cooled oscillator (with PLL) at two different temperatures (dots) with expected analytical distributions (lines). The distributions agree with the analytical prediction. b) Oscillator cooled with velocity damping. The experimental results agree with the analytical prediction. All experimental distributions and analytical predictions include a contribution from detection noise [42].

$$\rho(E)^{vd} = \frac{1}{Z_\alpha^{vd}} e^{-\frac{2E(\gamma_0 + \gamma_{fb})}{2\gamma_0 k_B T_0 + m\omega_0^2 S_{nn} \gamma_{fb}^2}} \quad (23)$$

$$\rho(E)^{PLL} = \frac{1}{Z_\alpha^{PLL}} e^{-\frac{E}{k_B T_0} (1 + \frac{G\omega_0}{2\gamma_0})} \quad (24)$$

where  $Z_\alpha^{vd}$  and  $Z_\alpha^{PLL}$  are the normalisation constants. Detection noise in the feedback signal has been included in the derivation of  $\rho(E)^{vd}$ . Both distributions still describe a Boltzmann-Gibbs distribution in contrast to an oscillator being cooled parametrically without a PLL which produces a highly non-thermal distribution [23]. Fig. 5. shows the energy distribution in units of  $k_B$  for both velocity damping and parametric feedback at different temperatures. These confirm that experimentally

the oscillator is still characterised by a Boltzmann-Gibbs distribution when cooled parametrically or with velocity damping. Due to the small SNR for small oscillator temperatures the distributions include some detection noise which manifests as an exponential distribution for white uncorrelated noise. Also shown are the expected distributions based on the measured temperature and detection noise. Our simulations suggest that as the SNR of the PLL becomes low the distribution will begin to deviate from the analytic result. This is because the phase error will be smaller for small SNR which is proportional to the oscillator energy. Therefore, larger energies will experience larger damping similar to the case of parametric feedback without a PLL [23]. However, detection noise in the experiment, which also has an exponential distribution, will make this deviation hard to measure.

## VIII. CONCLUSIONS

We have shown velocity damping is a more effective cooling scheme when compared to the parametric feedback using a PLL in an identical experimental situation. Our simulations have shown that this is fundamentally a result of the larger backaction in parametric feedback. Additional signals due to the  $x$ - and  $y$ -modes and higher order harmonics, an off-centre particle equilibrium position, and modulation of the particle frequency due to instabilities in the trap potential were all shown to heat the particle during parametric feedback with a PLL. These have no effect on the temperature from velocity damping since any additional signals from  $x$ - and  $y$ -modes do not couple to the  $z$ -mode, the force is applied in only one direction and therefore independent of position, and any modulation of the central frequency is automatically expressed in the feedback signal. Furthermore, for low-Q oscillators a Wiener filter will produce a better estimate of velocity than the delayed position method leading to lower CoM temperatures. Practically, parametric feedback is easier to implement in optical traps when compared to Paul traps since it requires modulation of only the trapping beam. Additionally, as the trapped particle will always be centred in the  $x - y$  plane of the optical potential, it is not affected by heating due to off-centre trapping in these directions. In a Paul trap, additional electrodes are required to cancel stray electric fields therefore velocity damping can be easily implemented in this scheme by applying the feedback signal to these electrodes. Lastly, unlike standard parametric cooling which leads to non-thermal energy distributions, both schemes studied here produce cold thermal distributions.

---

[1] U. Delić, M. Reisenbauer, K. Dare, D. Grass, V. Vuletić, N. Kiesel, and M. Aspelmeyer, “Cooling of a levitated nanoparticle to the motional quantum ground state,” *Science*, 2020.

[2] L. Magrini, P. Rosenzweig, C. Bach, A. Deutschmann-Olek, S. G. Hofer, S. Hong, N. Kiesel, A. Kugi, and M. Aspelmeyer, “Optimal quantum control of mechanical motion at room temperature: ground-state cooling.”

arXiv:2012.15188, 2020.

[3] F. Tebbenjohanns, M. Frimmer, V. Jain, D. Windey, and L. Novotny, “Motional sideband asymmetry of a nanoparticle optically levitated in free space,” *Phys. Rev. Lett.*, vol. 124, p. 013603, Jan 2020.

[4] J. Bateman, S. Nimmrichter, and K. e. a. Hornberger, “Near-field interferometry of a free-falling nanoparticle from a point-like source,” *Nat. Comm.*, vol. 5, no. 4788, 2014.

[5] C. Wan, M. Scala, G. W. Morley, A. A. Rahman, H. Ulbricht, J. Bateman, P. F. Barker, S. Bose, and M. S. Kim, “Free nano-object ramsey interferometry for large quantum superpositions,” *Phys. Rev. Lett.*, vol. 117, p. 143003, Sep 2016.

[6] S. Bose and G. W. Morley, “Matter and spin superposition in vacuum experiment.” arXiv:1810.07045, 2018.

[7] D. Goldwater, M. Paternostro, and P. F. Barker, “Testing wave-function-collapse models using parametric heating of a trapped nanosphere,” *Phys. Rev. A*, vol. 94, p. 010104, Jul 2016.

[8] A. Vinante, A. Pontin, M. Rashid, M. Toroš, P. F. Barker, and H. Ulbricht, “Testing collapse models with levitated nanoparticles: Detection challenge,” *Phys. Rev. A*, vol. 100, p. 012119, Jul 2019.

[9] G. Ranjit, M. Cunningham, K. Casey, and A. A. Geraci, “Zeptonewton force sensing with nanospheres in an optical lattice,” *Phys. Rev. A*, vol. 93, p. 053801, May 2016.

[10] V. Jain, J. Gieseler, C. Moritz, C. Dellago, R. Quidant, and L. Novotny, “Direct measurement of photon recoil from a levitated nanoparticle,” *Phys. Rev. Lett.*, vol. 116, p. 243601, Jun 2016.

[11] D. C. Moore, A. D. Rider, and G. Gratta, “Search for millicharged particles using optically levitated microspheres,” *Phys. Rev. Lett.*, vol. 113, p. 251801, Dec 2014.

[12] P. F. Barker and M. N. Shneider, “Cavity cooling of an optically trapped nanoparticle,” *Phys. Rev. A*, vol. 81, p. 023826, Feb 2010.

[13] D. E. Chang, C. A. Regal, S. B. Papp, D. J. Wilson, J. Ye, O. Painter, H. J. Kimble, and P. Zoller, “Cavity optomechanics using an optically levitated nanosphere,” *Proceedings of the National Academy of Sciences*, vol. 107, no. 3, pp. 1005–1010, 2010.

[14] O. Romero-Isart, A. C. Pflanzer, F. Blaser, R. Kaltenbaek, N. Kiesel, M. Aspelmeyer, and J. I. Cirac, “Large quantum superpositions and interference of massive nanometer-sized objects,” *Phys. Rev. Lett.*, vol. 107, p. 020405, Jul 2011.

[15] A. Ashkin and J. M. Dziedzic, “Optical levitation in high vacuum,” *Applied Physics Letters*, vol. 28, no. 6, pp. 333–335, 1976.

[16] N. Kiesel, F. Blaser, U. Delić, D. Grass, R. Kaltenbaek, and M. Aspelmeyer, “Cavity cooling of an optically levitated submicron particle,” *Proceedings of the National Academy of Sciences*, vol. 110, no. 35, pp. 14180–14185, 2013.

[17] J. Millen, P. Z. G. Fonseca, T. Mavrogordatos, T. S. Monteiro, and P. F. Barker, “Cavity cooling a single charged levitated nanosphere,” *Phys. Rev. Lett.*, vol. 114, p. 123602, Mar 2015.

[18] V. Jain, J. Gieseler, C. Moritz, C. Dellago, R. Quidant, and L. Novotny, “Direct measurement of photon recoil from a levitated nanoparticle,” *Phys. Rev. Lett.*, vol. 116, p. 243601, Jun 2016.

[19] J. Vovrosh, M. Rashid, D. Hempston, J. Bateman, M. Paternostro, and H. Ulbricht, “Parametric feedback cooling of levitated optomechanics in a parabolic mirror trap,” *J. Opt. Soc. Am. B*, vol. 34, pp. 1421–1428, Jul 2017.

[20] M. Poggio, C. L. Degen, H. J. Mamin, and D. Rugar, “Feedback cooling of a cantilever’s fundamental mode below 5 mK,” *Phys. Rev. Lett.*, vol. 99, p. 017201, Jul 2007.

[21] J. Gieseler, B. Deutscher, R. Quidant, and L. Novotny, “Subkelvin parametric feedback cooling of a laser-trapped nanoparticle,” *Phys. Rev. Lett.*, vol. 109, p. 103603, Sep 2012.

[22] V. Jain. PhD thesis, ETH, 2017.

[23] J. Gieseler, R. Quidant, C. Dellago, and L. Novotny, “Dynamic relaxation of a levitated nanoparticle from a non-equilibrium steady state,” *Nature Nanotechnology*, vol. 9, pp. 358–364, 2014.

[24] C. W. Hockney and J. W. Eastwood, “Computer simulation using particles,” 1984.

[25] J. Millen, T. Deesuwan, P. F. Barker, and J. Anders, “Nanoscale temperature measurements using non-equilibrium brownian dynamics of a levitated nanosphere,” *Nature Nanotechnology*, vol. 9, pp. 425–429, 2014.

[26] N. Wiener, “Extrapolation, interpolation, and smoothing of stationary time series: With engineering applications,” 1949.

[27] A. N. Kolmogorov *Bull. Acad. Sci. USSR Scr. Math.*, vol. 5, no. 3, 1941.

[28] F. Gardner, “Phaselock techniques, 2nd edition,” 1979.

[29] T. R. Albrecht, P. Grütter, D. Horne, and D. Rugar, “Frequency modulation detection using high-q cantilevers for enhanced force microscope sensitivity,” *Journal of Applied Physics*, vol. 69, no. 2, pp. 668–673, 1991.

[30] B. C. Buchler, M. B. Gray, D. A. Shaddock, T. C. Ralph, and D. E. McClelland, “Suppression of classic and quantum radiation pressure noise by electro-optic feedback,” *Opt. Lett.*, vol. 24, pp. 259–261, Feb 1999.

[31] A. J. Viterbi, “Phase-locked loop dynamics in the presence of noise by fokker-planck techniques,” *Proceedings of the IEEE*, vol. 51, no. 12, pp. 1737–1753, 1963.

[32] L. Ferialdi, A. Setter, M. Toroš, C. Timberlake, and H. Ulbricht, “Optimal control for feedback cooling in cavityless levitated optomechanics,” *New Journal of Physics*, vol. 21, p. 073019, jul 2019.

[33] D. J. Berkeland, J. D. Miller, J. C. Bergquist, W. M. Itano, and D. J. Wineland, “Minimization of ion micromotion in a paul trap,” *Journal of Applied Physics*, vol. 83, no. 10, pp. 5025–5033, 1998.

[34] D. Leibfried, R. Blatt, C. Monroe, and D. Wineland, “Quantum dynamics of single trapped ions,” *Rev. Mod. Phys.*, vol. 75, pp. 281–324, Mar 2003.

[35] N. P. Bullier, A. Pontin, and P. F. Barker, “Characterisation of a charged particle levitated nano-oscillator,” *Journal of Physics D: Applied Physics*, vol. 53, p. 175302, feb 2020.

[36] N. P. Bullier, A. Pontin, and P. F. Barker, “Super-resolution imaging of a low frequency levitated oscillator,” *Review of Scientific Instruments*, vol. 90, no. 9, p. 093201, 2019.

[37] E. Hebestreit, M. Frimmer, R. Reimann, C. Dellago, F. Ricci, and L. Novotny, “Calibration and energy measurement of optically levitated nanoparticle sensors,” *Review of Scientific Instruments*, vol. 89, no. 3, p. 033111,

2018.

[38] L. Dania, D. S. Bykov, M. Knoll, P. Mestres, and T. E. Northup, “Optical and electrical feedback cooling of a silica nanoparticle levitated in a paul trap,” *Phys. Rev. Research*, vol. 3, p. 013018, Jan 2021.

[39] P. Nagornykh, J. E. Coppock, B. E. Kane, P. Nagornykh, J. E. Coppock, and B. E. Kane, “Cooling of levitated graphene nanoplatelets in high vacuum Cooling of levitated graphene nanoplatelets in high vacuum,” vol. 244102, no. 2015, pp. 5–10, 2015.

[40] G. P. Conangla, A. W. Schell, R. A. Rica, and R. Quidant, “Motion control and optical interrogation of a levitating single nitrogen vacancy in vacuum,” *Nano Letters*, vol. 18, no. 6, pp. 3956–3961, 2018. PMID: 29772171.

[41] A. Pontin, N. P. Bullier, M. Toroš, and P. F. Barker, “Ultranarrow-linewidth levitated nano-oscillator for testing dissipative wave-function collapse,” *Phys. Rev. Research*, vol. 2, p. 023349, Jun 2020.

[42] N. P. Bullier, A. Pontin, and P. F. Barker, “Quadratic optomechanical cooling of a cavity-levitated nanosphere.” arXiv:2006.16103, 2020.

[43] J. Roberts and P. Spanos, “Stochastic averaging: An approximate method of solving random vibration problems,” *International Journal of Non-Linear Mechanics*, vol. 21, no. 2, pp. 111 – 134, 1986.

[44] E. Boujo and N. Noiray, “Robust identification of harmonic oscillator parameters using the adjoint fokker-planck equation,” *Proceedings of the Royal Society A: Mathematical, Physical and Engineering Sciences*, vol. 473, no. 2200, p. 20160894, 2017.